

THE INFLUENCE OF FILLER VOLUME FRACTION ON SENSITIVITY TO DISTRIBUTED STRAIN IN CARBON NANOFIBER/POLYURETHANE NANOCOMPOSITES

T. N. Tallman

Department of Mechanical Engineering
University of Michigan
Ann Arbor, MI, USA
ttallman@umich.edu

K. W. Wang

Department of Mechanical Engineering
University of Michigan
Ann Arbor, MI, USA
kwwang@umich.edu

ABSTRACT

Nanocomposites have unprecedented potential as smart, self-sensing materials for strain detection and tactile sensing. Filler volume fraction is an important consideration in the development of strain-sensitive nanocomposites because of its influence on sensitivity and dispersion uniformity. The influence of filler volume fraction is herein studied for its effect on the sensitivity of distributed strain detection via electrical impedance tomography in carbon nanofiber/polyurethane nanocomposites. It is found that lower volume fractions display the greatest sensitivity to strain; however, they also show the greatest variation in conductivity change indicating less uniform nanofiller dispersion.

KEYWORDS: nanocomposite, piezoresistivity, electrical impedance tomography, structural health monitoring, self-sensing

INTRODUCTION

Because their electrical conductivity depends on their mechanical state, nanocomposites have tremendous potential as high-sensitivity strain gauges [1-7] and for integrated damage detection [8-20]. Key to this potential is piezoresistivity. Piezoresistivity is rooted in the dependence of nanocomposite conductivity on well-connected nanofiller networks. That is, electrons traverse through nanofiller networks by tunneling between sufficiently proximate nanofillers. Strain that alters the connectivity of the network will also change the conductivity distribution of the nanocomposite, and damage that severs the network will manifest as a conductivity loss in the region of the damage.

Leveraging this for integrated damage detection has been studied by resistance change methods [11-14] and tomographic methods [15-20]. Resistance change methods measure the resistance between electrodes before and after damage and locate damage by interpolating resistance changes. Resistance change methods are computationally inexpensive, but require large electrode arrays. Tomographic methods such as electrical impedance tomography (EIT), conversely, require fewer electrodes located only along the periphery of the structure. EIT is more adept at spatially

resolving damage or strain, but it is also more computationally expensive. Compared to damage detection, however, less work has been done to investigate either resistance change or tomographic methods for strictly strain detection.

In addition to strain sensing for structural health monitoring (SHM) applications, highly compliant nanocomposites have potential for tactile sensing wherein it is necessary to spatially resolve points of contact. This capability is of keen interest to a growing number of robotic and biomedical applications. Locating contact within flexible planar skins has been approached by incorporating a sensing medium into a compliant matrix such that a grid is formed either by the sensing medium [21] or by line electrodes sandwiching the sensing medium [22]. Pressure-induced capacitance changes are then measured at the grid points so that pressure fields can be imaged by interpolating capacitance changes between measurement points. Despite the success of this approach, an important limitation is the dependence on a grid of sensors which is costly and complex to manufacture.

In light of the preceding discussion, we identify a novel approach for advancing the state of the art – employing EIT for strain sensing and tactile imaging. We herein explore this by examining the ability of EIT to accurately locate strain-induced conductivity changes and the influence of filler volume fraction on strain sensitivity in highly flexible carbon nanofiber (CNF)/polyurethane (PU) nanocomposites.

ELECTRICAL IMPEDANCE TOMOGRAPHY

EIT is a noninvasive method of imaging an internal conductivity distribution. Procedurally, the domain to be imaged is line with electrodes as shown in Figure 1. Current is injected between the first electrode pair and the resulting voltage measured between electrode pairs not actively involved in the current injection. The current injection is then moved around the domain such that every electrode pair receives an injection while the boundary voltages are continually collected.

EIT functions by minimizing the difference between a vector of the previously described boundary voltages and an analytical operator, known as the forward operator, which predicts the same boundary voltages as shown in Eq. (1).

$$\hat{\sigma} = \underset{\sigma}{\operatorname{argmin}} \|\mathbf{V}_m - \mathbf{F}(\sigma)\|^2 \quad (1)$$

Here, \mathbf{V}_m is the vector of experimentally collected voltages, $\mathbf{F}(\sigma)$ is the analytical operator that predicts the boundary voltages, and $\hat{\sigma}$ is a conductivity distribution satisfying the minimization. Next, perform a Taylor series expansion on $\mathbf{F}(\sigma)$ about some initial conductivity estimate, σ_0 , and retain only the linear terms as shown in Eq. (2).

$$\mathbf{F}(\sigma) \approx \mathbf{F}(\sigma_0) + \frac{\partial \mathbf{F}(\sigma_0)}{\partial \sigma} (\sigma - \sigma_0) \quad (2)$$

In order to proceed, we must next consider the forward operator. For steady-state diffusion, the relationship between currents and voltages is governed by Laplace's equation as shown in Eq. (3).

$$\nabla \cdot \sigma \nabla \phi = 0 \quad (3)$$

This is subjected to the complete electrode model boundary condition as shown in Eq. (4). This boundary condition assumes the electrodes are perfect conductors and that there is a voltage drop between the domain and the electrodes due to imperfect contact. Conservation of charge is also enforced by Eq. (5).

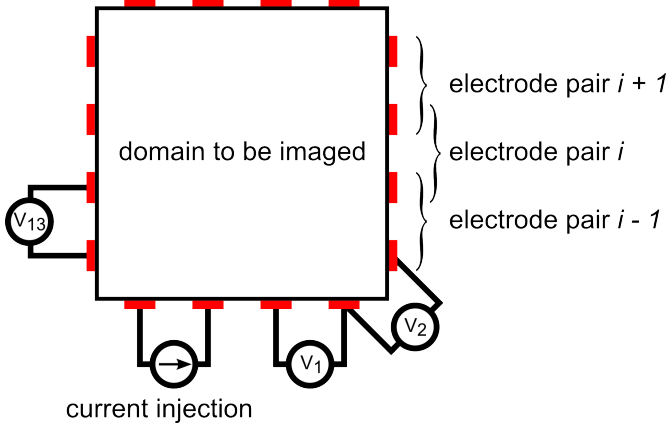


Figure 1. Representative EIT injection schematic shown with 16 electrodes.

$$\sigma \nabla \phi \cdot \mathbf{n} = \frac{1}{z_l} (V_l - \phi) \quad (4)$$

$$\sum_{l=1}^L \int_{E_l} \sigma \nabla \phi \cdot \mathbf{n} \, dS_l = 0 \quad (5)$$

In the preceding, ϕ is the domain solution, \mathbf{n} is the outward pointing normal vector, V_l is the voltage on the l th electrode, z_l is the contact impedance between the l th electrode and the domain, E_l is the length of the l th electrode, and L is the total number of electrodes.

The equations governing the forward operator are most expeditiously solved by finite element discretization as shown in Eq. (6).

$$\begin{bmatrix} \mathbf{A}_M + \mathbf{A}_Z & \mathbf{A}_W \\ \mathbf{A}_W^T & \mathbf{A}_D \end{bmatrix} \begin{bmatrix} \Phi \\ \mathbf{V} \end{bmatrix} = \begin{bmatrix} \mathbf{0} \\ \mathbf{I} \end{bmatrix} \quad (6)$$

$$A_{Zij} = \sum_{l=1}^L \int_{E_l} \frac{1}{z_l} w_i w_j \, dS_l \quad (7)$$

$$A_{Wli} = - \int_{E_l} \frac{1}{z_l} w_i \, dS_l \quad (8)$$

$$A_D = \operatorname{diag} \left(\frac{E_l}{z_l} \right) \quad (9)$$

In Eq. (6), \mathbf{A}_M is the standard diffusion stiffness matrix, and the remaining terms account for the additional degrees of freedom belonging to the electrodes and the contribution of contact impedances. w_i is the i th finite element interpolation function used on the electrodes.

Having discretized the forward operator, we substitute Eq. (2) into Eq. (1) as shown in Eq. (10).

$$\hat{\sigma} = \underset{\sigma}{\operatorname{argmin}} \|\mathbf{V}_e - \mathbf{J} \Delta \sigma\|^2 \quad (10)$$

Here, we have employed the substitutions $\mathbf{V}_e = \mathbf{V}_m - \mathbf{F}(\sigma_0)$, $\mathbf{J} = \partial \mathbf{F}(\sigma_0) / \partial \sigma$, and $\Delta \sigma = \sigma - \sigma_0$ and boldfaced quantities that have become vectors due to discretization. Recovering $\hat{\sigma}$ from Eq. (10), however, still is not straightforward because of the severe rank deficiency of \mathbf{J} . Tikhonov regularization is therefore employed to update $\hat{\sigma}$ iteratively as $\hat{\sigma}_{n+1} = \hat{\sigma}_n + \Delta \sigma$ where $\Delta \sigma$ is found as shown in Eq. (11).

$$\Delta \sigma = (\mathbf{J}^T \mathbf{J} + \alpha^2 \mathbf{L}^T \mathbf{L})^{-1} \mathbf{J}^T \mathbf{V}_e \quad (11)$$

This iterative update continues until the error is acceptably minimized. In this research the discrete Laplace operator is used for the regularization term, \mathbf{L} .

EXPERIMENTAL PROCEDURES

CNF/PU specimens are produced by colleagues at Penn State University (see acknowledgements) using ReoFlex 20 PU and Pyrograf III-PR-24-XT-HHT CNFs. Measured amounts of PU and CNFs are combined to produce composites at 7.5, 10.5, 12.5, and 15% filler volume fraction.

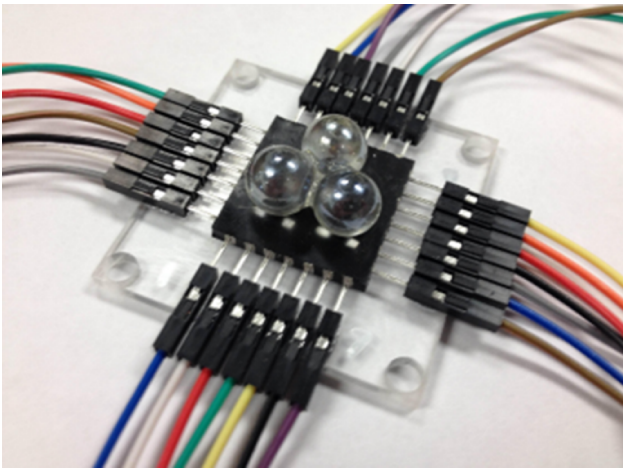


Figure 2. Experimental EIT setup including glass marbles to generate a strain field to be imaged by EIT.

Distributed strain is induced in $2.54 \text{ cm} \times 2.54 \text{ cm}$ CNF/PU samples by resting a 1.2 kg mass atop three bonded glass marbles as shown in Figure 2. Spherical glass marbles are used because they are non-conductive and their curvature does not cut into the soft CNF/PU. Three marbles are used to demonstrate the ability of EIT to clearly differentiate between multiple points of contact. A 28-electrode system is used to image strain-induced conductivity changes via an in-house EIT routine.

Electrodes are attached to the CNF/PU composites by first applying seven evenly spaced 1.59 mm patches of colloidal silver paste (TedPella 16032) per side. The paste is allowed to dry for at least one hour before jumper wires are pushed lightly into the patches and then glued to an acrylic (PMMA) base. An additional drop of silver paste is then applied where the jumper wire touches the originally applied patch to ensure good electrical contact. A Keithley 6221 current source is used to supply 2.5 mA DC injections between electrodes. Voltages are measured using two 16-channel National Instruments 6368-PXIe data acquisition cards for 10 s at 128 Hz. Data is collected via an in-house LabView code and smoothed using a moving average of half-width 256.

DISTRIBUTED STRAIN DETECTION VIA EIT

As shown in Figure 3, EIT accurately captures three distinct points of contact due to the spherical indenters for each volume fraction. Larger changes in conductivity are observed for lower volume fractions implying that they are more sensitive to the imposed strain fields. However, the EIT image produced for 7.5% filler volume fraction has a region in which the conductivity change is markedly larger. This is speculated to be due to non-uniform nanofiller dispersion and a region of lower nanofiller density in the vicinity of the region in question. Conversely, as the filler volume fraction increases, such deviations are less pronounced. Conductivity increases in the region of the distributed load indicating that the nanofillers are becoming closer together thereby

decreasing the tunneling resistance felt by electrons. Additionally, the compression increases the density of the nanofiller network thereby increasing the number of viable tunneling junctions. These factors combine resulting in a net increase in conductivity.

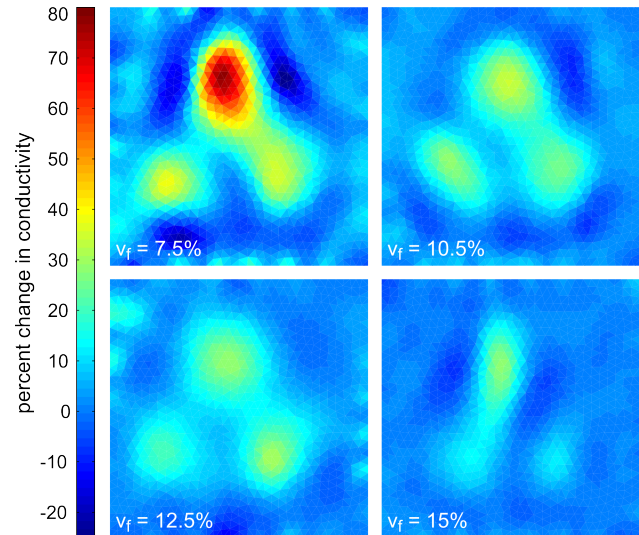


Figure 3. Distributed strain sensing results. EIT clearly captures three points of contact for each volume fraction.

SUMMARY AND CONCLUSIONS

Herein we have investigated employing CNF/PU nanocomposites and EIT for distributed strain sensing. Conductivity changes induced by bonded glass marbles are successfully imaged by EIT, and the point of contact of each marble is clearly discerned. Furthermore, it is found that sensitivity to distributed strain increases with decreasing filler volume fraction. However, the lowest volume fraction also shows the greatest variation in conductivity change potentially indicating less uniform dispersion. Nonetheless, all volume fractions accurately locate strain-induced conductivity changes thereby demonstrating the potential of distributed strain sensing via nanocomposites and EIT.

ACKNOWLEDGMENTS

This research is partially supported by the US Army Research Office (W911NF-10-1-00267) and the National Science Foundation (CMMI-DS-1232436).

The authors gratefully thank Dr. Sila Gungor and Professor Charles E. Bakis of the Pennsylvania State University for producing the CNF/PU.

REFERENCES

1. Hu N, Masuda Z, Yamamoto G, Fukunaga H, Hashida T, Qiu J. 2008, "Effect of fabrication process on electrical properties of polymer/multi-wall carbon nanotube

- nanocomposites”, *Composites Part A: Applied Science and Manufacturing*, Vol(39), pp. 893-903.
2. Hu N, Karube Y, Yan C, Masuda Z, Fukunaga H. 2008, “Tunneling effect in a polymer/carbon nanotube nanocomposite strain sensor”, *Acta Materialia*, Vol(56), pp. 2929-2936.
 3. Hu N, Karube Y, Arai M, Watanabe T, Yan C, Li Y, et al. 2010, “Investigation on sensitivity of a polymer/carbon nanotube composite strain sensor”, *Carbon*, Vol(48), pp. 680-687.
 4. Kang I, Schulz MJ, Kim JH, Shanov V, Shi D. 2006, “A carbon nanotube strain sensor for structural health monitoring”, *Smart Materials and Structures*, Vol(15), pp. 737.
 5. Loh KJ, Kim J, Lynch JP, Kam NWS, Kotov NA. 2007, “Multifunctional layer-by-layer carbon nanotube-polyelectrolyte thin films for strain and corrosion sensing”, *Smart Materials and Structures*, Vol(16), pp. 429-438.
 6. Loh KJ, Lynch JP, Shim BS, Kotov NA. 2008, “Tailoring piezoresistive sensitivity of multilayer carbon nanotube composite strain sensors”, *Journal of Intelligent Material Systems and Structures*, Vol(19), pp. 747-764.
 7. Tallman T, Wang KW. 2013, “An arbitrary strains carbon nanotube composite piezoresistivity model for finite element integration”, *Applied Physics Letters*, Vol(102), pp. 011909.
 8. Gao L, Chou TW, Thostenson ET, Zhang Z. 2010, “A comparative study of damage sensing in fiber composites using uniformly and non-uniformly dispersed carbon nanotubes”, *Carbon*, Vol(48), pp. 3788-3794.
 9. Gao L, Chou TW, Thostenson ET, Zhang Z, Coulaud M. 2011, “In situ sensing of impact damage in epoxy/glass fiber composites using percolating carbon nanotube networks”, *Carbon*, Vol(49), pp. 3382-3385.
 10. Thostenson ET, Chou TW. 2006, “Carbon Nanotube Networks: Sensing of Distributed Strain and Damage for Life Prediction and Self-Healing”, *Advanced Materials*, Vol(18), pp. 2837-2841.
 11. Naghashpour A, Hoa SV. 2013, “A technique for real-time detection, location and quantification of damage in large polymer composite structures made of electrically non-conductive fibers and carbon nanotube networks”, *Nanotechnology*, Vol(24), pp. 455502.
 12. Naghashpour A, Hoa SV. 2015, “A technique for real-time detecting, locating, and quantifying damage in large polymer composite structures made of carbon fibers and carbon nanotube networks”, *Structural Health Monitoring*, Vol(14), pp. 35-45.
 13. Zhang D, Ye L, Wang D, Tang Y, Mustapha S, Chen Y. 2012, “Assessment of transverse impact damage in GF/EP laminates of conductive nanoparticles using electrical resistive tomography”, *Composites: Part A*, Vol(43), pp. 1587-1598.
 14. Viets C, Kaysser S, Schulte K. 2014, “Damage mapping of GFRP via electrical resistance measurements using nanocomposite epoxy matrix systems” *Composites: Part B*, Vol(65), pp. 80-88.
 15. Hou TC, Loh KJ, Lynch JP. 2007, “Spatial conductivity mapping of carbon nanotube composite thin films by electrical impedance tomography for sensing applications”, *Nanotechnology*, Vol(18), pp. 315501.
 16. Loh KJ, Hou TC, Lynch JP, Kotov NA. 2009, “Carbon nanotube sensing skins for spatial strain and impact damage identification”, *Journal of Nondestructive Evaluation*, Vol(28), pp. 9-25.
 17. Loyola BR, Briggs TM, Arronche L, Loh KJ, La Saponara V, O'Bryan G, et al. 2013, “Detection of spatially distributed damage in fiber-reinforced polymer composites”, *Structural Health Monitoring*, Vol(12), pp. 225-239.
 18. Tallman TN, Gungor S, Wang KW, Bakis CE. 2014, “Damage detection and conductivity evolution in carbon nanofiber epoxy via electrical impedance tomography”, *Smart Materials and Structures*, Vol(23), pp. 045034.
 19. Tallman TN, Gungor S, Wang KW, BCE. 2015, “Damage Detection via Electrical Impedance Tomography in Glass Fiber/Epoxy Laminates with Carbon Black Filler”, *Structural Health Monitoring*, Vol(14), pp. 100-109.
 20. Kim B, Lu Y, Kim T, Han JW, Meyyappan M, Li J. 2014, “Carbon Nanotube Coated Paper Sensors for Damage Diagnosis”, *ACS Nano*, Vol(8), pp. 12092-12097.
 21. Lipomi DJ, Vosgueritchian M, Tee BCK, Hellstrom SL, Lee JA, Fox CH, et al. 2011, “Skin-like pressure and strain sensors based on transparent elastic films of carbon nanotubes”, *Nature Nanotechnology*, Vol(6), pp. 788-792.
 22. Mannsfeld SCB, Tee BCK, Stoltenberg RM, Chen CVHH, Barman S, Muir BVO, et al. 2010, “Highly sensitive flexible pressure sensors with microstructured rubber dielectric layers”, *Nature Materials*, Vol(9), pp. 859-864.